

Fission time scale from pre-scission neutron and α multiplicities in the $^{16}\text{O} + ^{194}\text{Pt}$ reaction

K. Kapoor, S. Verma, P. Sharma, R. Mahajan, N. Kaur, G. Kaur, B. R. Behera, K. P. Singh, and A. Kumar^{*}
Department of Physics, Panjab University, Chandigarh 160014, India

H. Singh
Department of Physics, Kurukshetra University, Kurukshetra-136119, India

R. Dubey, N. Saneesh, A. Jhingan, and P. Sugathan
Inter University Accelerator Centre, New Delhi-110067, India

G. Mohanto, B. K. Nayak, and A. Saxena
Nuclear Physics Division, Bhabha Atomic Research Centre, Mumbai-400085, India

H. P. Sharma
Department of Physics, Banaras Hindu University, Varanasi-221005, India

S. K. Chamoli
Department of Physics and Astrophysics, University of Delhi, Delhi-110007, India

I. Mukul
Department of Particle Physics and Astrophysics, Weizmann Institute of Science, Rehovot-76100, Israel

V. Singh
Department of Physics, Punjab Technical University, Jalandhar-144603, India

(Received 29 April 2017; revised manuscript received 11 October 2017; published 20 November 2017)

Pre- and post-scission α -particle multiplicities have been measured for the reaction $^{16}\text{O} + ^{194}\text{Pt}$ at 98.4 MeV forming ^{210}Rn compound nucleus. α particles were measured at various angles in coincidence with the fission fragments. Moving source technique was used to extract the pre- and post-scission contributions to the particle multiplicity. Study of the fission mechanism using the different probes are helpful in understanding the detailed reaction dynamics. The neutron multiplicities for this reaction have been reported earlier. The multiplicities of neutrons and α particles were reproduced using standard statistical model code JOANNE2 by varying the transient (τ_{tr}) and saddle to scission (τ_{ssc}) times. This code includes deformation dependent-particle transmission coefficients, binding energies and level densities. Fission time scales of the order of $50\text{--}65 \times 10^{-21}$ s are required to reproduce the neutron and α -particle multiplicities.

DOI: [10.1103/PhysRevC.96.054605](https://doi.org/10.1103/PhysRevC.96.054605)

I. INTRODUCTION

The study of fusion-fission dynamics is one of the interesting areas of heavy-ion-induced nuclear reactions. Depending upon the excitation energy, temperature, and various other factors, the compound nucleus may tend towards the fission process. Fusion-fission dynamics of the excited nucleus can be studied by characterizing the emitted particles, such as α , p , ν , and γ during the course of deexcitation [1,2]. Fission time scale measurements are carried out by measuring the multiplicities of neutrons [3,4], charged particles [2,5,6], and giant dipole resonance (GDR) [7] emitted during fusion-fission. Fission time is divided into two major parts, the transient time (τ_{tr}) and the saddle to scission time (τ_{ssc}). The study of fission time scale gives insight into fission dynamics [8]. It has been

reported earlier that the fission process slows down to an order ($10^{-20}\text{--}10^{-19}$ s) due to nuclear viscosity [9].

Various theories have been formulated to elucidate the nature and magnitude of nuclear viscosity [10]. The standard statistical model was found to be insufficient to reproduce the measured particle multiplicities and the fission lifetimes [11]. Based on this observation, Kramer modified the Bohr-Wheeler's standard statistical model pointing toward the longer fission lifetime due to which higher particle emission is expected [12]. Measured excessive particle emission indicates the hindrance in the fission process. To discern the fission process, emission of the particles is divided into two major components. Particles emitted from the compound nucleus are called pre-scission particles whereas the particles emitted from the fragments are called post-scission particles [5]. The contribution of the pre- and post-scission particles in the measured spectra can be extracted using the moving source analysis. Investigation of the emitted particles provides paramount facts on the dynamical and statistical aspects of

^{*}Corresponding author: ashok@pu.ac.in

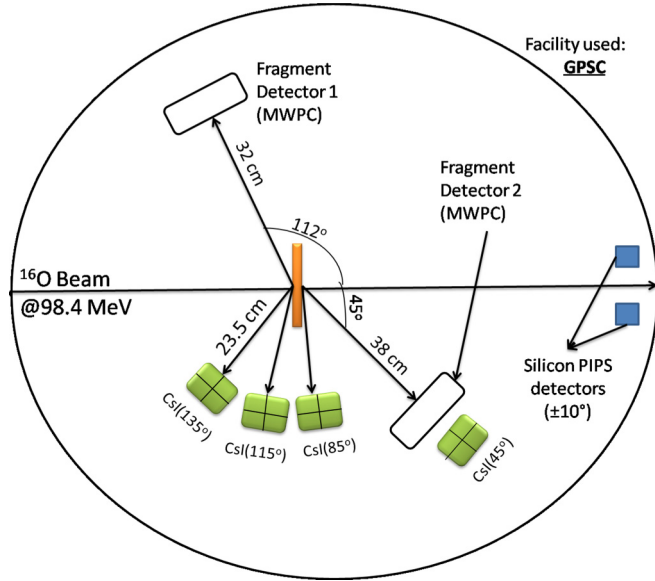


FIG. 1. Schematic diagram of experimental setup representing fission detectors as MWPC 1 and 2 kept at folding angle and charged particle detectors CsI(Tl) kept at 45° , 85° , 115° , and 135°

fission process [6]. The study of a reaction using different probes can give clearer picture about the fission dynamics. Subjected to fission, large kinematic focusing occurs during the separation of two nuclei at the scission point, which plays an important role in the fission dynamics [13]. The charged particles multiplicities (proton and α) can provide more information on the dynamics of fission process due to the occurrence of Coulomb barrier at the exit channel [14], which is absent in case of neutrons. It has been observed [2,5] that α -particle emission also takes place very near the neck region just before the scission. This part of the pre-scission α particle emitted near the neck region is termed as near-scission emission (NSE). Although, there have been many studies on the pre-scission α -particle emission in heavy ion fusion-fission reactions, still there is a scarcity of data for the NSE in these reactions.

Neutron multiplicity for $^{16}\text{O} + ^{194}\text{Pt}$ reaction at 98.4 MeV has been reported earlier [4], which indicates that the fission process is dissipative in nature at high excitation energy of the compound nucleus. To understand more deeply the dynamics involved in the fission of ^{210}Rn nucleus, in the present work we measured the α -particle multiplicity for this reaction at the same excitation energy. To get the fission time scales, standard statistical model code JOANNE2 is used, which also incorporates the effect of change in particle binding energy with deformation. The results from JOANNE2 have been compared to experimentally obtained values.

Section II gives the details about the experimental setup and the detector systems used. Section III describes details about the moving source fitting procedure for the α -particle spectra to deduce the α_{Pre} , α_{Post} , and α_{NSE} , contributions. Sections IV and V describe the details of the dynamical model calculation using the HICOL code and the standard statistical model analysis to obtain the fission time scale using the JOANNE2 code, respectively, followed by summary.

II. EXPERIMENTAL DETAILS

The experiment was performed with 15UD Pelletron facility at Inter University Accelerator Centre (IUAC), New Delhi, using General Purpose Scattering Chamber (GPSC). A self-supporting enriched target of ^{194}Pt having a thickness of 1.7 mg/cm^2 was used in the experiment. A beam of ^{16}O at energy 98.4 MeV, was bombarded on ^{194}Pt to form ^{210}Rn compound nucleus at the excitation energy of 61 MeV. Multiwire proportional counter (MWPC) detectors were used for the detection of fission fragments. The MWPC detector was made up of four electrodes: anode, cathode, and position signals [15]. Two MWPC detectors were kept at the folding angles so as to detect complementary fission fragments. One of the MWPC detectors was kept at an angle of 45° with respect to (w.r.t.) beam at a distance of 38 cm from the center of the target, whereas the second MWPC detector was kept at an angle of 112° w.r.t. beam at a distance of 32 cm from the center of the target. These MWPC detectors had an active area of $(20 \text{ cm} \times 10 \text{ cm})$. Two passivated implanted planar silicon (PIPS) detectors were also placed inside the scattering chamber at $\pm 10^\circ$ as monitors. The detector system used in current setup has sixteen CsI(Tl) crystals, each having an area of $20 \text{ mm} \times 20 \text{ mm}$ with thickness of 3 mm. The crystals in group of four, forming a solid angle of 7.3 msr, were kept at 45° , 85° , 115° , and 135° w.r.t. the beam direction at a distance of 23.4 cm.

CsI(Tl) has the intrinsic property of discriminating between different types of particles such as α , protons, deuterons, tritons, and γ photons. In order to differentiate between different particles, ballistic deficit pulse shaping technique was used to obtain two decay times: long decay time (τ_L) and short decay time (τ_S). Plotting long decay time to short decay time gives bands corresponding to different particles as shown in Fig. 2. The details of the procedure are given in our previous publication [16].

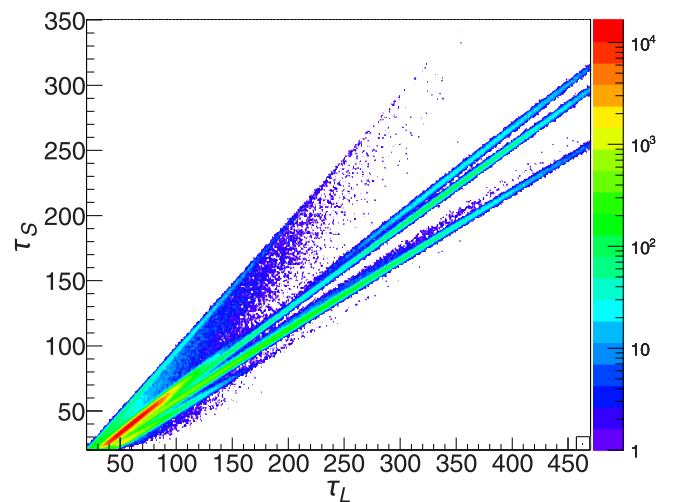


FIG. 2. Two-dimensional plot of long shaping time (τ_L) vs short shaping time (τ_S), representing different bands corresponding to different particles. γ from photodiode are seen in the top band, Second and third band represents protons and deuterons, respectively, whereas the bottom band represents α particles.

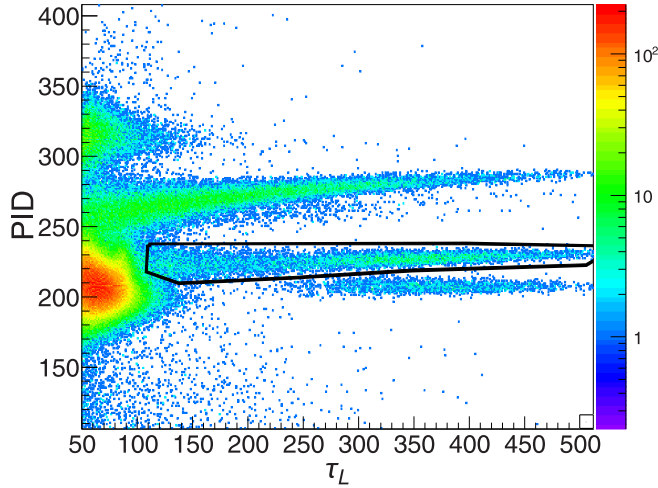


FIG. 3. Particle identification plot with PID on Y axis and long shaping time (τ_L) on X axis. Black-marked band represents the α -particles band

The particle identification (PID) plot was obtained by taking the difference between τ_L and τ_S divided by τ_L .

$$PID = \frac{\tau_L - \tau_S}{\tau_L}. \quad (1)$$

A two-dimensional view of the obtained spectra is shown in Fig. 3.

Energy calibration of the CsI(Tl) detector for α particles was performed using ^{254}Am and ^{229}Th sources giving α energies up to 8 MeV. To take care of the nonlinear behavior for α particles at high energies, the in-beam calibration of the CsI(Tl) detector was also performed using $^{12}\text{C}(^{12}\text{C},\alpha)^{20}\text{Ne}^*$ and $^7\text{Li}(^{12}\text{C},\alpha)^{15}\text{N}^*$ reactions at 30 MeV and 20 MeV, respectively, which provide discrete α energies ranging from 5 MeV–25 MeV corresponding to ^{20}Ne , ^{15}N states. During the in-beam calibration, all the four CsI(Tl) detectors were brought near beam axis at $\pm 10^\circ$ and $\pm 20^\circ$ to minimize the kinematic broadening.

For data collection, events were recorded by OR gating between the fission detector and charged particle detector. A TAC signal was generated by giving start from the OR gating of anodes of two MWPC and stop from the CsI(Tl) detector. Fission-gated α spectra were obtained by normalizing with total fission after correcting for random coincidence.

III. DATA ANALYSIS

The dynamical models proposed in the early 1980s predicted the onset of the quasifission process for heavier systems when product $Z_p Z_t \geq 1600$. The experimental signature of the quasifission was reported by Hinde *et al.*, [17,18] in a system having even much lower $Z_p Z_t$. One of the experimental signatures of the quasifission is the broadened mass ratio distribution [19]. The mass ratio distribution for $^{16}\text{O} + ^{194}\text{Pt}$ reaction was studied using the formula given below [20].

$$M_R = \frac{M_2}{M_1 + M_2}, \quad (2)$$

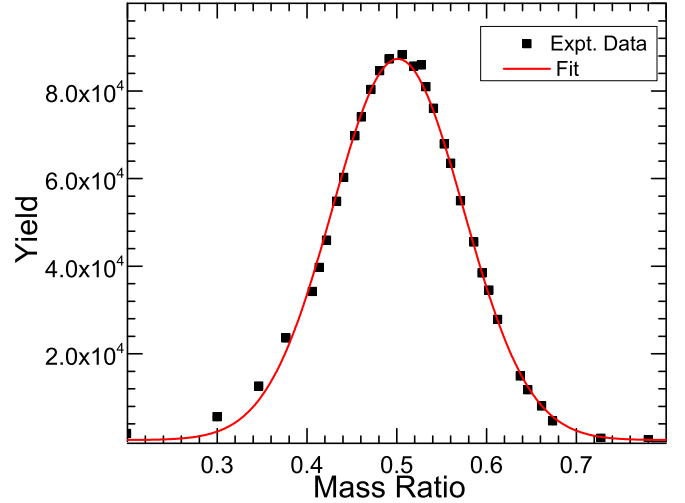


FIG. 4. Fission fragments mass ratio distribution at $E_{\text{lab}} = 98.4$ MeV. The distribution is symmetric and centered at 0.5. Solid line is the Gaussian fit to the experimental mass ratio distribution.

where M_1 and M_2 are the masses of complementary fission fragments. As shown in Fig. 4, the mass ratio distribution peaks at 0.5 representing the symmetric fission and contribution for a noncompound process is negligible. The large angular opening of MWPC fission detector was divided into four equal parts during the off-line data analysis in order to have the better angle definitions. Each slicing had a bin size of $\approx 7.5^\circ$ forming various angles w.r.t. beam as well as CsI(Tl) detector. Different values of relative angles, i.e., the angle of the α -particle detector w.r.t. beam (Θ_α), the angle of the α -particle detector w.r.t. fission detector (MWPC 1) ($\Theta_{\alpha f1}$), and the angle of the α -particle detector w.r.t. another fission detector (MWPC 2) ($\Theta_{\alpha f2}$) were generated. The angles of CsI detectors with respect to beam and MWPCs are given in Table I. Final α -particle multiplicity spectra were obtained at various angles by dividing the coincidence spectra with the total fission counts and the solid angle of the detector. In total, eight combinations for (Θ_α), ($\Theta_{\alpha f1}$), and ($\Theta_{\alpha f2}$) were obtained.

The normalized α -particles spectra, thus obtained, were fitted simultaneously with a moving source model considering four sources namely: compound nucleus, complementary fission fragments, and the near-scission emission (NSE). In

TABLE I. Various angles corresponding to four slices made in MWPC during off-line analysis, values of angles are in degrees.

S. No	Θ_α	$\Theta_{\alpha f1}$	$\Theta_{\alpha f2}$
1	115	73.6	127.3
2	115	66.3	134.8
3	115	81.5	119.9
4	115	58.9	142.6
5	135	101	99.9
6	135	93.6	107.3
7	135	86.1	114.6
8	135	78.6	122

the moving source analysis, symmetric fission is assumed, which is confirmed from Fig. 4, and mean values of fragment mass and charge are used. The α -particles emission is assumed to be isotropic in the rest frames of sources and energy spectra are calculated using the constant temperature level density expression [5] given below,

$$n(\epsilon) \approx \alpha_p \epsilon \sigma(\epsilon) \exp\left(\frac{-\epsilon}{T}\right), \quad (3)$$

where α_p and ϵ are the multiplicity and the energy of the emitted α particles in the rest frame, T is the temperature of the source, and $\sigma(\epsilon)$ is the inverse reaction cross section. The inverse reaction cross section was calculated using Wong's formula [21].

$$\sigma(\epsilon) = \frac{\hbar \omega R^2}{2\epsilon} \log \left\{ 1 + \exp \left[\frac{2\pi}{\omega} (\epsilon - V_B) \right] \right\}, \quad (4)$$

where $\hbar \omega$ is the curvature of fusion barrier for angular momentum (ℓ) = 0. The pre- and post-scission values for $\hbar \omega$ used in moving source analysis were 4.8 and 4.0 MeV, respectively [5]. Temperature (T) for the pre- and post-scission sources was calculated using the formula:

$$T = \sqrt{\frac{E^*}{a}}, \quad (5)$$

where E^* is the intrinsic excitation energy of the source and a represents the level density parameter, which was taken as $A/11$ for the compound nucleus and $A/7$ for the fission fragments [5]. The values for T_{pre} and T_{post} were calculated to be 1.52 MeV and 1.1 MeV respectively after scaling down T_{pre} by a factor of 11/12 to account for the multistep evaporation [14]. The Coulomb barrier for α particles (V_B) at the exit channel was calculated using the following expression [22]:

$$V_B = \frac{1.44 Z_P (Z_S - Z_P)}{r_0 [(A_P)^{1/3} + (A_S - A_P)^{1/3}] + \delta} \text{ MeV}, \quad (6)$$

where A_P , Z_P and A_S , Z_S are the masses and charges of the α particle and emitting sources, respectively. The value of r_0 was taken as 1.45 fm. The parameter δ was used to care for the reduction in barrier due to the deformation effects of the sources and was taken as 2.0 for compound nucleus and 0.4 for the fission fragments. The values of $V_{\text{pre}}^B = 20.2$ MeV, and $V_{\text{post}}^B = 12.7$ MeV were used in moving source code for pre- and post-scission sources, respectively. The study of NSE of α particles is important for understanding the collective fission dynamics and can provide valuable information on the scission point characteristics. This emission is assumed to take place at scission point almost similar to the ternary fission at low energy. It is well established in low-energy fission that NSE has an energy distribution, which is nearly Gaussian, and an angular distribution, which has a noticeable dependence on the energy of the emitted particles [6]. Since the mechanism of NSE α particles in heavy-ion reactions is still not clear, for simplicity we have assumed that both the energy and the angular distribution have Gaussian forms and are independent of each other. Therefore, in order to extract the NSE contribution to α -particle spectra in the moving source analysis, the energy and angular distribution were assumed to

be Gaussian in the rest frame and the following expression was used [2]:

$$\eta(\epsilon, \theta) \approx \alpha_{NSE} \exp \left[\frac{-(\epsilon - \epsilon_P)^2}{2\sigma_\epsilon^2} \right] \exp \left[\frac{-(90 - \theta)^2}{2\sigma_\theta^2} \right], \quad (7)$$

where α_{NSE} is the α -particle multiplicity of the NSE, ϵ_P is the peak or mean energy of α particle, θ is the relative angle of α particle w.r.t. scission axis, σ_ϵ is the standard deviations of the energy distribution, and σ_θ is the width of angular distribution in the rest frame. Near scission emission is assumed to be dominating in perpendicular direction to scission axis.

The α -particle spectra from four sources were calculated in rest frame using the equations (3), (4), and (7) and then were converted to laboratory frames using the appropriate Jacobians. The spectra thus obtained from the individual four sources were summed up to have total α spectra. The mean fragment velocities were determined using Viola's systematic [23] for the total kinetic energy released in fission process. The temperatures (T_{pre} , T_{post}) and Coulomb barriers (V_{pre}^B and V_{post}^B) were fixed during the moving source analysis to extract the pre-scission, post-scission, and NSE contributions. The pre-scission, post-scission, and NSE multiplicities were kept as free parameters during the fitting. Figure 5 shows fitted spectra for the individual sources along with total spectra at various angles. Various contributions are marked with different color schemes. Values of the multiplicities obtained from the best fit are $\alpha_{\text{pre}} = (9.1 \pm .29) \times 10^{-3}$, $\alpha_{\text{post}} = (0.62 \pm .08) \times 10^{-3}$, and $\alpha_{NSE} = (0.22 \pm .03) \times 10^{-3}$, $\epsilon_P = 20.0 \pm 0.2$ MeV, $\sigma_\epsilon = 2.4 \pm 0.3$ MeV, and $\sigma_\theta = 11.5^\circ \pm 1.5^\circ$, having a minimum value of $\chi^2/(\text{degree of freedom}) = 2.63$. In these values of multiplicity, systematic errors have not been included. One of the main sources of systematic errors in the multiplicity may be the temperature. In the present paper, we have used the level density parameter $a = A/11$ taken from the work of Gupta *et al.* [5]. In the literature, however, this parameter has also been taken as $A/10$. We found that if level density parameter is taken $A/10$, then the multiplicity increases by $\approx 10\%$. Moreover it can be seen in Fig. 5, that the neck emission is more dominant where the angle between fission fragment and the emitted charged particle is approaching towards 90° , whereas it decreases at smaller angles. This is due to the Coulomb focusing in the perpendicular direction.

IV. DYNAMICAL MODEL CALCULATIONS

Fusion-fission reaction is a dynamic process of high complexity and many partial waves contribute to dynamically evolving mononucleus. In these reactions, only for the lower partial waves, the colliding system gets trapped in the minimum of the potential energy surface behind the saddle and lead to the formation of a true compound nucleus. For higher partial waves, the observed fissionlike reactions have to be related to processes that are not completely equilibrated. In the dynamical model developed by Feldmeier [24], coupling between the intrinsic and the collective degrees of freedom is treated in a microscopic picture of particle exchange, which provides the friction and the diffusion tensor. The dynamical evolution of the two colliding nuclei is described by a sequence

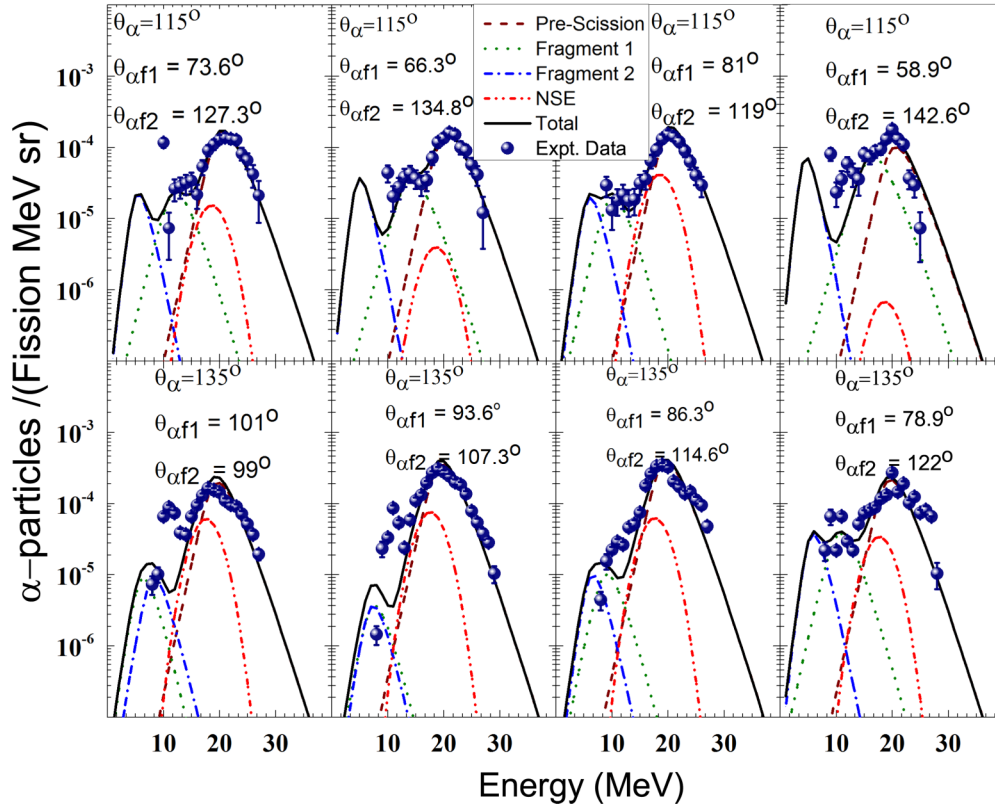


FIG. 5. Normalized α -particle multiplicity spectra along with fits of moving source formula. These spectra are shown at various relative angles between the CsI detectors and the fission detectors in laboratory frame. Various contributions are represented in different colors. Green (dotted) and blue (dash-dotted) line represents the contribution from two fragments or post-scission segment whereas the brown (dashed) line is representing the compound nucleus contributions or pre-scission segment and the neck contribution is represented by red (dash-dot-dot) line or near scission emission. The error bars represent the statistical errors only.

of shapes, which basically consist of two spheres connected by a conical neck. Throughout the collision, the volume of the shape is conserved so that the uniform mass and charge densities remain the same. The macroscopic shapes of the nuclear system are represented by axially symmetric configurations with sharp surfaces. To get the information about the shape evolution of colliding nuclei, dynamical model calculations were performed using the code HICOL [24]. This code gives detailed information about the sequences of the shape change between the two nuclei and the neck formation when the fragments are about to separate each other. In general terms, the code uses mainly three parameters:

- (i) the distance between the two nuclei (s);
- (ii) the neck coordinate (σ)

$$\sigma = \frac{V_0 - \frac{4\pi}{3}R_1^3 - \frac{4\pi}{3}R_2^3}{V_0}; \quad (8)$$

- (iii) the mass asymmetry (Δ)

$$\Delta = \left[\frac{R_1 - R_2}{R_1 + R_2} \right]. \quad (9)$$

Where V_0 is the total volume of the system, R_1 and R_2 are the radii of two colliding nuclei. In addition, there are three rotational degrees of freedom (intrinsic and relative) of the

dinuclear complex. Using these sets of shape and rotational coordinates, their evolution is followed by solving Langevin equations of motion. One-body dissipation is assumed to be the predominant mechanism for these types of reactions in this energy range. The HICOL program accounts separately for the amount of excitation energy associated with the thermal, deformation, and rotational energy, and the maximum angular momentum contributing to the formation of equilibrated compound nucleus. The evolution of the dissipation energy with various angular momentum for $^{16}\text{O} + ^{194}\text{Pt}$ forming ^{210}Rn , is shown in Fig. 6. It is seen that the time required to attain the asymptotic value of the dissipation energy is increasing with increasing ℓ .

In Fig. 7, the elongation of the fusing nuclei is plotted as a function of time. The calculations were performed for the wide range of ℓ values. Since the compound nucleus is formed for the trajectories that are trapped in the potential well, it is imperative that for the higher ℓ values trajectories do not lead to an equilibrated compound nucleus. For this reaction the calculated maximum angular momentum (ℓ_{max}) is $\approx 38\hbar$ and HICOL predicts that all the trajectories up to ℓ_{max} are contributing to the complete fusion of the system. This again confirms that the contribution from the noncompound process is negligible.

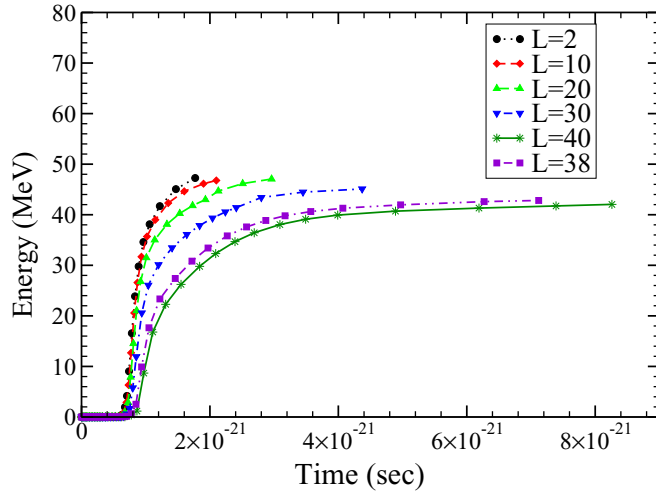


FIG. 6. Dissipation energy as a function of time for various values of angular momentum.

V. STATISTICAL MODEL CALCULATIONS

Statistical model calculations were carried out using the code JOANNE2 [8] to reproduce measured particle multiplicities α_{pre} and ν_{pre} . This code incorporates the deformation-dependent particle binding energies and transmission coefficients. Pre-scission particle emission is assumed to take place from two points in deformation space corresponding to mean presaddle deformation (Z_{tr}) and mean saddle-to-scission deformation (Z_{ssc}). Z represents the elongation of the symmetry axis (in units of the diameter of the spherical nucleus). Presaddle emission takes place over the region from equilibrium to saddle. The code JOANNE2 allows particle emission from only nearly spherical systems for mean pre-saddle time (τ_{tr}) and then allows fission decay to compete with particle emission for mean saddle-to-scission time (τ_{ssc}). The level density (a) parameters for spherical compound nucleus a_n and a_{ssc} at each Z_{ssc} for the saddle to scission

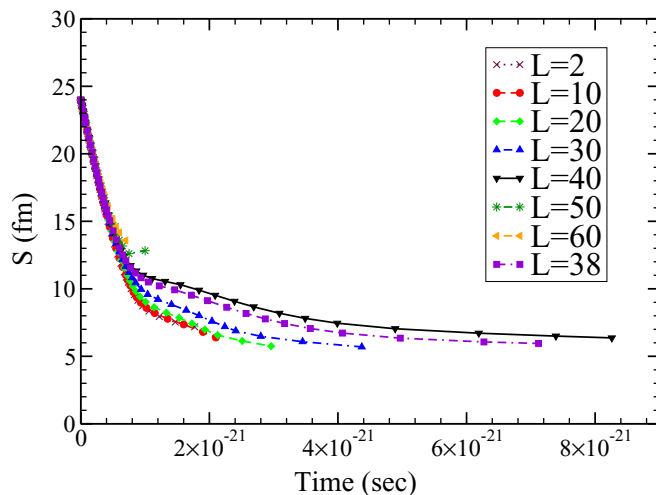


FIG. 7. Dinucleus elongation as a function of time for various values of angular momentum.

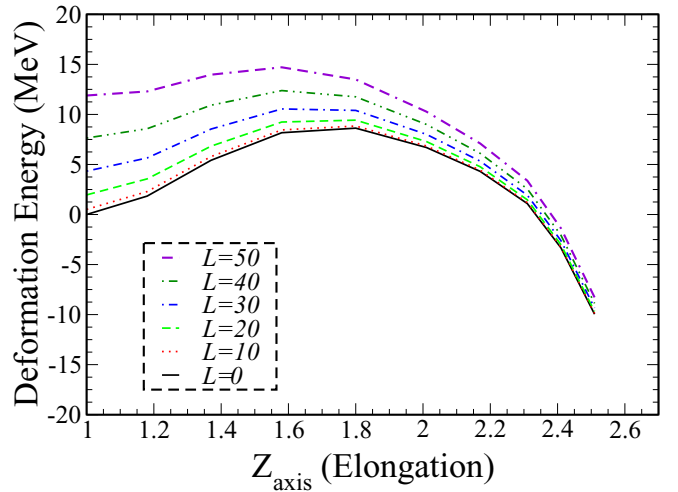


FIG. 8. Potential energy diagram ^{210}Rn , representing the deformation energy as a function of elongation for various angular momentum values.

are calculated in JOANNE2 using the formalism of Toke and Swiatecki [9]. Calculations are performed by varying either Z_{ssc} or mean saddle-to-scission time (τ_{ssc}) to study its effect on particle multiplicity. The variation of potential energy with deformation for $^{16}\text{O} + ^{194}\text{Pt}$ for various angular momenta (ℓ) is shown in Fig. 8. From this figure, the saddle-to-scission emitter can be assumed having Z_{ssc} values in the range 1.90–2.45.

The variation of binding energies with deformation is shown in Fig. 9, for compound nucleus ^{210}Rn . It can be seen from the figure that particle binding energy for charged particles (proton and α) increases whereas for neutron it decreases.

We tried to reproduce the measured ν_{pre} and α_{pre} values with different combinations of τ_{tr} and τ_{ssc} independently for different values of Z_{ssc} . Figure 10, shows τ_{tr} versus τ_{ssc}

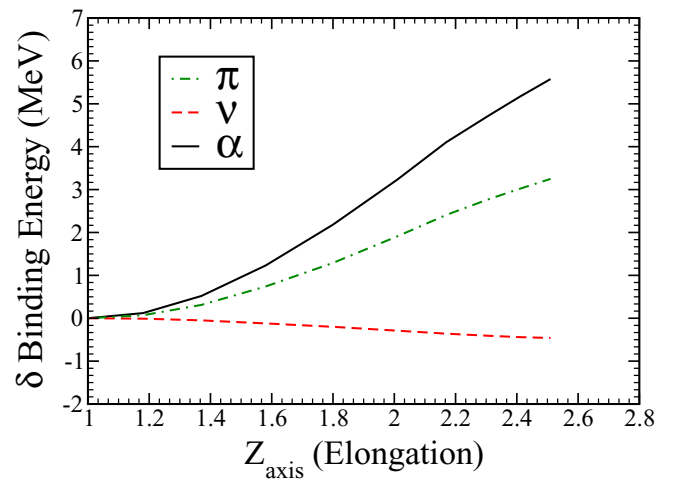


FIG. 9. Deformed liquid drop model predictions of the deviation of binding energies from spherical nucleus for ν -, π -, and α -particle emission

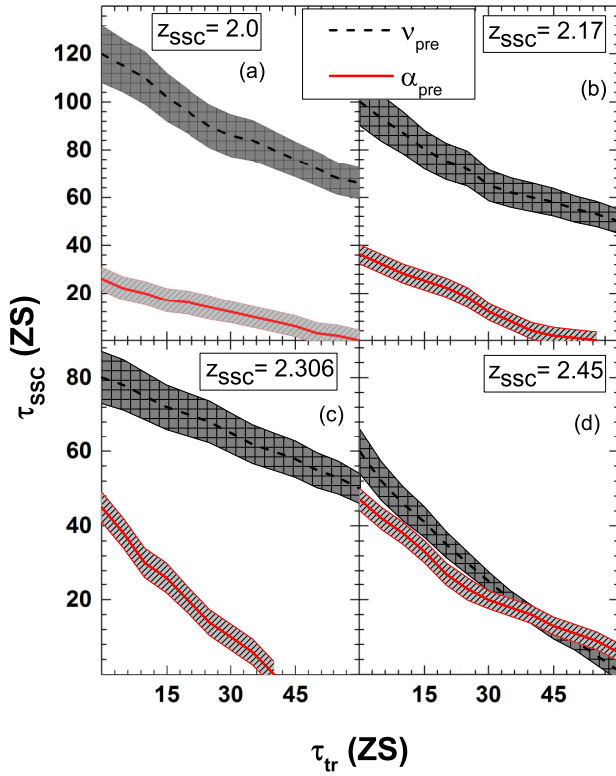


FIG. 10. τ_{tr} - τ_{ssc} plot from JOANNE2 for various Z_{ssc} deformation values required to reproduce experimental ν_{pre} , and α_{pre} are shown in black and red, respectively. (a) $Z_{ssc} = 2.0$, (b) $Z_{ssc} = 2.17$, (c) $Z_{ssc} = 2.3$, and (d) $Z_{ssc} = 2.4$, and corresponding particle emission.

plots for three different values of Z_{ssc} . In Fig. 10(a), it can be seen that for $Z_{ssc} = 2.0$, large total fission time scale ($\tau_{tot} \approx 120$ zs) ($1 \text{ zs} = 10^{-21} \text{ s}$) is required to explain ν_{pre} , however, a smaller $\tau_{tot} \approx 30$ zs is required to explain α_{pre} . In Fig. 10(b), for $Z_{ssc} = 2.17$, which represents more elongation, smaller time ($\tau_{tot} \approx 100$ zs) is required to reproduce the ν_{pre} and $\tau_{tot} \approx 40$ zs is required to explain α_{pre} . However Fig. 10(c), for $Z_{ssc} = 2.3$, ($\tau_{tot} \approx 80$ zs) is required to reproduce the ν_{pre} and $\tau_{tot} \approx 45$ zs is required to explain α_{pre} . This change is observed because neutron binding energy decreases with deformation as shown in Fig. 9 and smaller τ_{ssc} is required to reproduce the ν_{pre} . In case of α , binding energy increases with increasing deformation and the combination of binding energy and emission barrier decides the variation of the τ_{ssc} with Z_{ssc} . In Fig. 10(d), values for deformation were kept fixed at $Z_{ssc} = 2.45$, near to scission point, and the values obtained to explain α_{pre} and ν_{pre} are quite near to each other and an overlap between the two was found to be around $\tau_{tot} \approx (50-65)$ zs. Calculations have also been performed by varying Z_{ssc} and τ_{ssc} to observe their effect on ν_{pre} and α_{pre} . Calculations for ν_{pre} and α_{pre} for fixed Z_{tr} at 1.31 and $\tau_{tr} = 20$ zs as function of $Z_{ssc} = 2.4$ are shown in Fig. 11. It is seen that the value of ν_{pre} and α_{pre} increases with increasing τ_{ssc} . It can be seen in Figs. 11(a) and 11(c) that the experimentally obtained multiplicity for neutron and α can be easily reproduced by varying τ_{ssc} . Figures 11(b) and 11(d) represent the pre-scission α and neutron multiplicity, respectively, as a function of

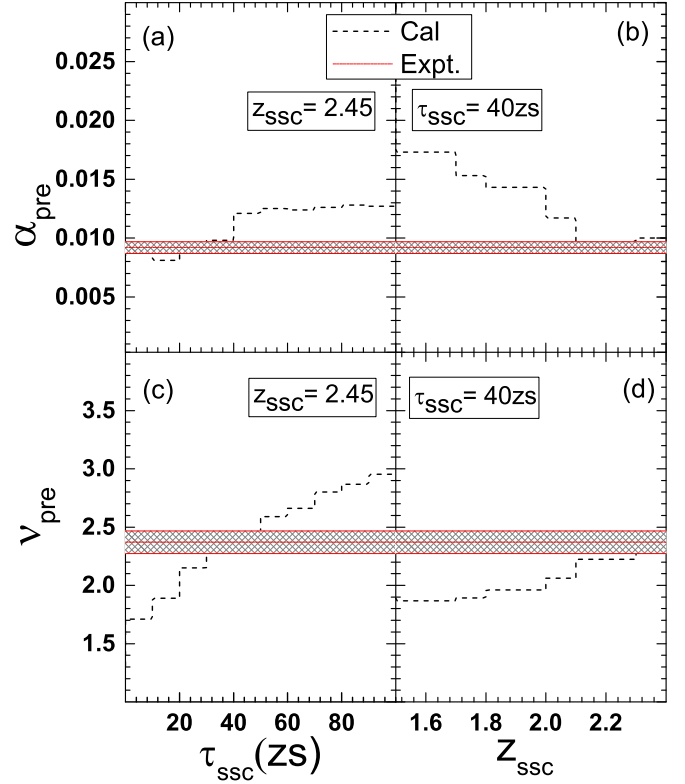


FIG. 11. The variation of ν_{pre} and α_{pre} as a function τ_{ssc} in (a) and (c) and as a function of Z_{ssc} in (b) and (d) for $^{16}\text{O} + ^{194}\text{Pt}$. The shaded region corresponds to value of ν_{pre} and α_{pre} .

deformation in saddle to scission. The experimentally obtained value is shown as red band. The experimental ν_{pre} is taken from Sandal *et al.* [4]. Pre-scission neutron multiplicity is seen to be increasing with the more elongation whereas pre-scission α multiplicity is seen to decrease with increasing elongation justifying the change in particle binding energy with increasing deformation represented in Fig. 9. A clear overlap between the experimental value and calculated value is seen.

In one of the earlier reports by Gupta *et al.* [5], a systematic study for various reactions have been performed and it is seen that the α_{pre} normalized to excitation energy ($E_{CN}^{2,3}$) as a function of α -particle emission Q value, for various projectile-target combinations shows a linear trend. The α_{pre} value obtained from the reaction under study was also normalized to excitation energy ($E_{CN}^{2,3}$) as a function of α -particle emission Q value. It is observed that α_{pre} too follows the similar trend.

VI. SUMMARY AND CONCLUSION

In the present paper, we have measured the charged particle multiplicity for $^{16}\text{O} + ^{194}\text{Pt}$ reaction at 98.4 MeV forming ^{210}Rn nucleus. Charged particles were measured in coincidence with the fission fragments. Fitting of the α -particles spectra was performed with moving source code in order to extract the α particles pre-scission, post-scission, and near-scission multiplicities. It was assumed that the pre-scission emission takes place for two points in the deformation space. Results were compared with statistical model code

JOANNE2 to obtain α -particles multiplicity. We found that both the neutron and α -particle multiplicity can be reproduced using JOANNE2 code, if we assume that both are emitted near $Z_{ssc} = 2.45$, which gives $\tau_{total} = (50-65)$ zs. It is seen that the α_{pre} value normalized to excitation energy ($E_{CN}^{2,3}$) as a function of α -particle emission Q value follows the same trend as reported earlier. Thus the fission lifetime obtained for this system is (50–65) zs.

ACKNOWLEDGMENTS

The authors would like to thank pelletron accelerator staff of IUAC, New Delhi for providing beam of excellent quality during the whole experiment. The authors are also grateful to Dr. A. Chatterjee for the valuable suggestions and discussion on various aspects during the analysis. One of the authors, K.K., is also thankful of Inter University Accelerator Center (IUAC), New Delhi for providing financial assistance.

-
- [1] D. J. Hinde, R. J. Charity, G. S. Foote, J. R. Leigh, J. O. Newton, S. Ogaza, and A. Chatterjee, *Nucl. Phys. A* **452**, 550 (1986).
- [2] K. Ramachandran, A. Chatterjee, A. Navin, K. Mahata, A. Shrivastava, V. Tripathi, S. Kailas, V. Nanal, R. G. Pillay, A. Saxena *et al.*, *Phys. Rev. C* **73**, 064609 (2006).
- [3] A. Chatterjee, A. Navin, S. Kailas, P. Singh, D. C. Biswas, A. Karnik, and S. S. Kapoor, *Phys. Rev. C* **52**, 3167 (1995).
- [4] R. Sandal, B. R. Behera, V. Singh, M. Kaur, A. Kumar, G. Singh, K. P. Singh, P. Sugathan, A. Jhingan, K. S. Golda *et al.*, *Phys. Rev. C* **87**, 014604 (2013).
- [5] Y. K. Gupta, D. C. Biswas, R. K. Choudhury, A. Saxena, B. K. Nayak, B. John, K. Ramachandran, R. G. Thomas, L. S. Danu, B. N. Joshi *et al.*, *Phys. Rev. C* **84**, 031603 (2011).
- [6] J. P. Lestone, J. R. Leigh, J. O. Newton, D. J. Hinde, J. X. Wei, J. X. Chen, S. Elfstrom, and M. Zielinska-Pfabe, *Nucl. Phys. A* **559**, 277 (1993).
- [7] N. P. Shaw, I. Diszegi, I. Mazumdar, A. Buda, C. R. Morton, J. Velkovska, J. R. Beene, D. W. Stracener, R. L. Varner, M. Thoennessen *et al.*, *Phys. Rev. C* **61**, 044612 (2000).
- [8] J. P. Lestone, *Phys. Rev. Lett.* **70**, 2245 (1993).
- [9] J. Toke and W. J. Swiatecki, *Nucl. Phys.* **29**, 462 (1962).
- [10] H. Ikezoe, N. Shikazono, Y. Nagame, Y. Sugiyama, Y. Tomita, K. Ideno, I. Nishinaka, B. J. Qi, H. J. Kim, A. Iwamoto *et al.*, *Phys. Rev. C* **46**, 1922 (1992).
- [11] N. Bohr and J. A. Wheeler, *Phys. Rev.* **56**, 426 (1939).
- [12] H. Kramers, *Physica* **7**, 284 (1940).
- [13] D. J. Hinde, H. Ogata, M. Tanaka, T. Shimoda, N. Takahashi, A. Shinohara, S. Wakamatsu, K. Katori, and H. Okamura, *Phys. Rev. C* **39**, 2268 (1989).
- [14] Y. K. Gupta, D. C. Biswas, B. John, B. K. Nayak, A. Chatterjee, and R. K. Choudhury, *Phys. Rev. C* **86**, 014615 (2012).
- [15] A. Jhingan, P. Sugathan, K. S. Golda, R. P. Singh, T. Varughese, H. Singh, B. R. Behera, and S. K. Mandal, *Rev. Sci. Instrum.* **80**, 123502 (2009).
- [16] A. Jhingan, P. Sugathan, G. Kaur, K. Kapoor, N. Saneesh, T. Banerjee, H. Singh, A. Kumar, B. R. Behera, and B. K. Nayak, *Nucl. Instrum. Methods Phys. Res., Sect. A* **786**, 51 (2015).
- [17] D. J. Hinde, M. Dasgupta, J. R. Leigh, J. P. Lestone, J. C. Mein, C. R. Morton, J. O. Newton, and H. Timmers, *Phys. Rev. Lett.* **74**, 1295 (1995).
- [18] D. J. Hinde, M. Dasgupta, J. R. Leigh, J. C. Mein, C. R. Morton, J. O. Newton, and H. Timmers, *Phys. Rev. C* **53**, 1290 (1996).
- [19] A. W. Fairhall, *Phys. Rev.* **102**, 1335 (1956).
- [20] K. Kapoor, A. Kumar, N. Kaur, B. R. Behera, K. P. Singh, V. Singh, G. Kaur, P. Sharma, R. Mahajan, H. Singh *et al.*, *Proc. DAE-BRNS symposium on Nuclear Physics* **59**, 572 (2014).
- [21] C. Y. Wong, *Phys. Rev. Lett.* **31**, 766 (1973).
- [22] R. Yanez, T. A. Bredeweg, E. Cornell, B. Davin, K. Kwiatkowski, V. E. Viola, R. T. de Souza, R. Lemmon, and R. Popescu, *Phys. Rev. Lett.* **82**, 3585 (1999).
- [23] V. E. Viola, K. Kwiatkowski, and M. Walker, *Phys. Rev. C* **31**, 1550 (1985).
- [24] H. Feldmeier, *Rep. Prog. Phys.* **50**, 915 (1987).